Article

Low-Temperature Removal of Dissociated Bromine by Silicon Atoms for an On-Surface Ullmann Reaction

Kewei Sun, Tomohiko Nishiuchi, Keisuke Sahara, Takashi Kubo, Adam S. Foster, and Shigeki Kawai*

Read Online

ACCESS | Metrics & More | Article Recommendations | Supporting Information

ABSTRACT: On-surface Ullmann-type reactions are widely used to fabricate various carbon nanostructures in a bottom-up approach by conjugating small hydrocarbons via dehalogenation. In the reaction, the dissociated halogen atoms remain on the substrate and are usually removed by high-temperature annealing. Here, we demonstrate an alternative method in which most of bromine atoms can be desorbed from Au(111) just by depositing silicon atoms. A combination of scanning tunneling microscopy and density functional theory calculations revealed that the highly volatile silicon tetrabromine is synthesized and consequently desorbs from the surface even at room temperature. This low-temperature removal of the halogen atoms may increase flexibility in on-surface chemical reactions toward synthesis and characterization of further functionalized carbon nanomaterials.
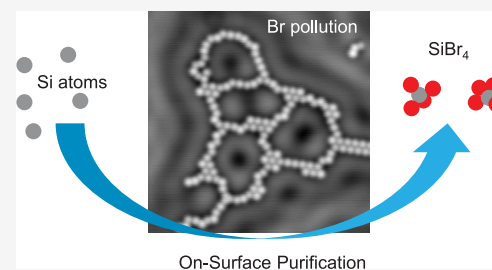
I. INTRODUCTION

Since the first systematic synthesis of conjugated porphyrin blocks on a surface,[1] on-surface chemical reactions have attracted tremendous attention of researchers in the fields of chemistry, physics, and surface science. The structures of synthesized nanocarbon materials can be controlled at the atomic scale by precursor molecules. Molecules are usually deposited on metal surfaces and are in situ conjugated by various on-surface chemical reactions, such as the Ullmann reaction,[1−3] Bergmann reaction,[4,5] Glaser reaction,[6−8] Sonogashira cross coupling,[9] Heck cross coupling,[10] Schiff base reaction,[11] dehydration,[12] dehydrogenation,[13,14] decarboxylation,[15] and so on. Among them, the Ullmann reaction became popular, especially after the successful synthesis of graphene nanoribbons (GNRs)[16] combined with subsequent cyclodehydrogenation.[17] In the reaction, halo-substituted precursors are thermally deposited on metal surfaces in vacuum. Then, the C−X (X = Cl, Br, I) σ bonds in halo-substituted molecules are cleaved by annealing the substrate. The reaction temperature is strongly affected by the species of the halogen atom[18] and the catalysis of surface metal atoms[19] as well as the structures of precursors.[20] Consequently, the precursors are conjugated with each other by C−C homo-coupling.[21]

In the Ullmann reaction, dissociated halogen atoms usually remain on the surfaces at the reaction temperature. Their electronegativity leads to binding to synthesized hydrocarbons[22] and consequently condensing them.[23] This phenomenon often hinders the diffusion of molecules, and if excessive, the growth of the polymer can potentially be disturbed.[24−26] The electronic properties of nanostructures are also affected by the condensed halogen atoms.[27,28] Therefore, it is of importance to remove halogen atoms from surfaces. So far, thermal desorption of the halogen atoms at temperatures

higher than 300 °C is commonly used.[22,25,29,30] In general, Br atoms are absent in most GNR synthesis processes since the temperature for cyclodehydrogenation is usually higher than that for the thermal desorption of Br atoms.[16,31−33] Nevertheless, since high-temperature annealing is not required for synthesis of oligomers[21] and narrow GNRs (for instance, $n = 5$ GNR),[34] it is still beneficial to develop a technique to remove the dissociated Br atoms at lower temperatures. Furthermore, high-temperature annealing might lead to random fusion of carbon nanomaterials.[35] To this end, Abyazisani et al. recently demonstrated that the exposure of atomic hydrogen for 6 min with a pressure of 5×10^{-7} mbar leads to the removal of Br atoms from a copper surface.[36] However, since the highly reactive atomic hydrogen produces sp^3 carbon compounds as well as contaminations on the surface, the sample has to be annealed at 275 °C to complete the removal process. Therefore, it is still beneficial to develop a technique to remove the Br atoms at mild and totally UHV-compatible conditions.

Here, we report low-temperature removal of Br atoms from Au(111) by depositing Si atoms with a combination of scanning tunneling microscopy (STM) and density functional theory (DFT) calculations. Abundant Br atoms were produced via synthesis of $n = 5$ GNR with 1,4,5,8-tetrabromonaphthalene (TBN) molecules.[34] We found that highly volatile

silicon tetrabromide ($SiBr_4$) molecules are synthesized on the surface even at room temperature and are consequently desorbed. The remaining Br atoms were mostly removed by gentle annealing at 180 °C.

■ II. METHODS

A. Experimental Section. All measurements were performed with a homemade low-temperature STM/atomic force microscopy system, operating in ultrahigh vacuum at 4.3 K. A chemically etched tungsten tip was used as a probe. A clean Au(111) surface was prepared by repeated cycles of Ar^+ sputtering for 10 min (1×10^{-6} mbar, 1000 eV) and annealing at 760 K for 10 min. TBN molecules were in situ deposited onto the substrate held at room temperature. The sample was subsequently heated at 180 °C for 10 min to synthesize GNRs as well as produce Br atoms via debromination. Si atoms were deposited on the substrate held at room temperature (SPECS, single-pocket electron beam evaporator). A hat-like shaped Au(111) sample was mounted on an OMICRON-type sample plate. For the chemical reaction, the sample was indirectly heated via the backside of the sample plate with a tungsten filament (no electron beam heating). The temperature of the sample was measured with a thermocouple, which is contacted to the edge of the sample plate. In order to reduce the thermal gradient, the sample was heated relatively slowly. We assume that the error in the temperature measurement at 200 °C is less than 10 °C.

B. Theoretical Calculation. All first-principles calculations in this work were performed using the periodic plane-wave basis VASP code 4,[37,38] implementing the spin-polarized DFT. To accurately include van der Waals interactions in this system, we used the many-body dispersion energy method.[39,40] Projected augmented wave potentials were used to describe the core electrons[41] with a kinetic energy cutoff of 550 eV (with PREC = accurate). The systematic k-point convergence was checked for all systems with sampling chosen according to the system size. This approach converged the total energy of all the systems to the order of millielectronvolts. The properties of the bulk and surface of Au were carefully checked within this methodology, and excellent agreement was achieved with experiments. For calculations of the molecules on the surface, a vacuum gap of at least 1.5 nm was used. The upper three layers of Au (five layers in total) and all atoms in the molecules were allowed to relax to a force of less than 0.01 eV/Å. Note that several molecular adsorption configurations were considered before deciding on the lowest energy structure. For adsorption of isolated Br on the Au(111) surface, our results agree with previous experimental and theoretical studies.[42,43] All energies mentioned are with reference to relaxed total energies. Atomic structure visualizations were made with the VMD package.[44] Simulated STM images were calculated at a constant current with parameters from experiments using the HIVE package[45] based on the Tersoff−Hamann approximation.[46]

■ III. RESULTS AND DISCUSSION

We employed TBN ($C_{10}H_4Br_4$) molecules to produce Br atoms and $n = 5$ GNRs following previous studies (Figure 1a).[34] An annealing temperature of 180 °C is high enough to synthesize GNRs and low enough to leave dissociated Br atoms on Au(111) since no cyclodehydrogenation is required. This precursor is suitable to produce abundant Br atoms since four Br atoms are substituted into the small precursor
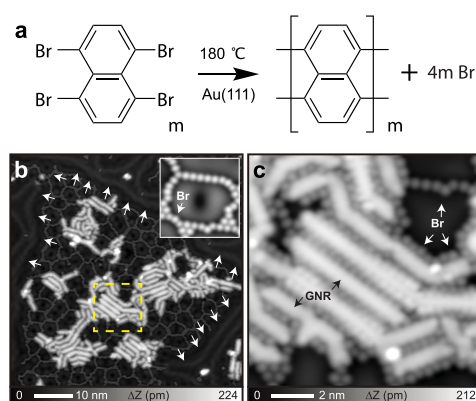
Figure 1. (a) $n = 5$ GNR synthesis with TBN molecules on Au(111). (b) Large-scale STM topography of Au(111) taken after the formation of GNRs. The deformed herringbone structures are indicated by arrows. Inset shows a close view of the Br network. (c) Close-up view of an area indicated by a square in (b). GNRs are condensed via Br atoms. Measurement parameters: sample bias voltage $V = 200$ mV and tunneling current $I = 5$ pA in (b), $V = 100$ mV and $I = 100$ pA in inset of (b), and $V = 20$ mV and $I = 100$ pA in (c).

molecule. Figure 1b shows a large-scale STM topography in which several GNRs are condensed with each other. Furthermore, the herringbone reconstruction of Au(111) is observed only at the area where both GNR and Br are absent, as indicated by arrows. Thus, the surface reconstruction was quenched by the halogen atoms, which is in agreement with previous studies.[47] The porous network is composed of a number of Br atoms aligned with a gap of 0.50 ± 0.01 nm (inset of Figure 1b).[48] The well-confined surface state indicates strong chemisorption of the Br atom to the substrate (2.4 eV in our simulations, Figure S1). Figure 1c shows a close-up view of the area indicated by a square in Figure 1b in which the Br atoms locate around the GNRs. Attraction between the electronegative Br and the electropositive hydrogen of the hydrocarbon[49] is responsible for the condensation of GNRs. Note that if the population of GNRs further increases, dissociated Br atoms will cover the entire surface, leading to unstable imaging conditions (Figure S2).

Initially, we attempted to measure the intrinsic electronic property of $n = 5$ GNR by electronic decoupling between GNR and Au(111). To this end, we deposited Si atoms to form a gold silicide buffer under the GNRs.[50] Figure 2a shows the large-scale STM topography after depositing Si atoms on Au(111) at room temperature. Interestingly, the Br network no longer exists, although the irregular reconstruction is still seen. Apparently, the deposited Si atoms removed the Br atoms from the surface. Since one-dimensional Br condensation is still observed along the herringbone structure, it can readily be concluded that the amount of deposited Si atoms (∼0.02 ML) was not sufficient to remove all Br atoms as well as to form the gold silicide buffer. Hereafter, we focus on the low-temperature removal of Br atoms by Si atoms. We found that the modulation of the herringbone structure is affected by the formation of clusters; since the apparent height of the cluster (∼150 pm) is larger than that for the Br atoms (∼80 pm), the cluster is most probably a Si−Br complex (inset of Figure 2a). However, the observed STM topography alone cannot tell the detailed structure. It is known that $SiBr_4$ is highly volatile (boiling point: 153 °C at 1 atm), and it is probable that four Br
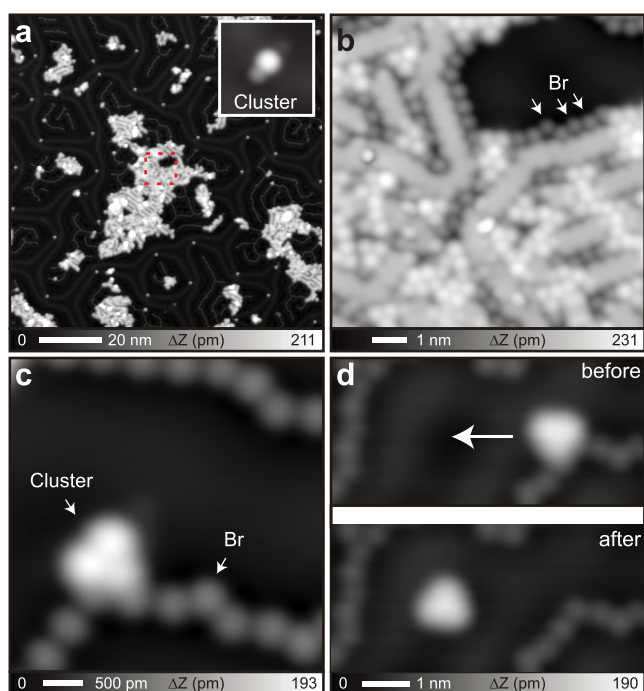
Figure 2. (a) STM topography taken after depositing Si atoms on Au(111) at room temperature. Inset shows a close-up view of a cluster attached to the elbow site of the herringbone structure. (b) Close-up view of the area indicated by a square in (a). (c) Close-up view of the Br line structure with a large cluster. (d) Tip-induced manipulation of the large cluster. Measurement parameters: $V = 200$ mV and $I = 10$ pA in (a), $V = 10$ mV and $I = 50$ pA in (b), $V = 50$ mV and $I = 100$ pA in (c), and $V = 200$ mV and $I = 10$ pA in (d).

atoms can be desorbed from the surface as a $SiBr_4$ compound. Therefore, the $SiBr_x$ ($x = 1,2,3$) cluster seen at the elbow site is likely an intermediate. Note that a similar desorption based on the silyl group was also found in the reaction with a precursor with TMS groups.[8] While the volatility of $SiBr_4$ is high enough for it to desorb from Au(111) at room temperature, the diffusion of Si and/or Br atoms seems to be insufficient. Figure 2b shows the area of high GNR concentration: the side-by-side assembly due to the Br atoms is reduced, and the GNRs are positioned rather randomly. The binding energy to the electropositive hydrogen at the edges of GNRs may prevent the diffusion of the Br atom, resulting in insufficient formation of $SiBr_4$. Figure 2c shows the STM topography of a large cluster attached to the Br line structure. Since we observed three maxima in the cluster, we assume that this cluster corresponds to $SiBr_3$. Interestingly, the cluster can be moved by the STM tip while avoiding any damage to the Br line structure (Figure 2d). This local probe manipulate indicates a relatively low diffusion barrier of the cluster, which may be responsible for the further reaction to form $SiBr_4$. Nevertheless, our statistical analysis revealed that the quantities of Br atoms in the area (where GNRs were absent) before and after Si deposition are approximately 1.1 and 0.3 nm^{-2}, respectively. In other words, 70% of Br atoms was removed by this process (1916 Br atoms to 528 Br atoms in the analyzed area of 1800 nm^2). This analysis suggests that the deposited Si atoms reacted with Br atoms at room temperature and $SiBr_4$ molecules were synthesized. In contrast to the strong chemisorption of Br atom on Au(111), its high volatility leads to desorption from the surface.

In order to enhance the diffusion of Br and Si on the surface, we heated the sample at 180 °C as well as deposited further Si atoms. Note that the annealing temperature is comparable to that for the Ullmann reaction on Au(111). After this process, the condensed Br atoms on the terrace are no longer observed (Figure 3a). Furthermore, the GNRs become isolated on the
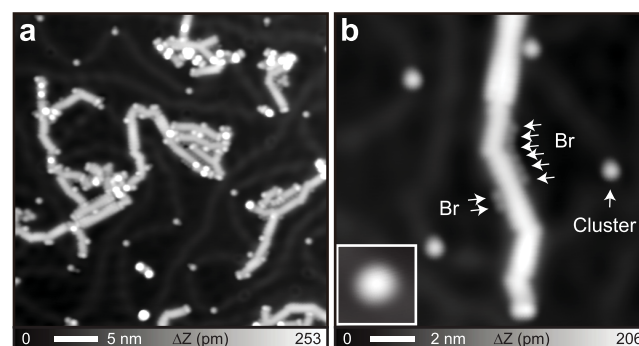
Figure 3. (a) STM topography taken after heating at 180 °C. (b) Close-up view of an isolated GNR. Inset shows a cluster. Measurement parameters: $V = 100$ mV and $I = 20$ pA in (a), $V = 50$ mV and $I = 100$ pA in (b).

surface as their condensation is barely seen. Figure 3b shows an example of a single GNR, which is macroscopically polygonal-chain-shaped. We deduce that this fusion event is mainly related to the high reactivity of the zigzag edge. In fact, such a random fusion is also seen in the synthesis of GNRs by heating at above 300 °C without Si atoms (Figure S3). We found only eight Br atoms attached to the armchair edge of the GNR in the image. The bright spots at the elbow site of the herringbone structure correspond to the $SiBr_x$ cluster (inset of Figure 3b), and Br atoms no longer exist on the flat terrace except at the GNR site. In some cases, larger clusters can also be found at the elbow site. Nevertheless, the results demonstrate that enhanced diffusion from the gentle annealing induces further reduction of the Br atoms on Au(111). Note that the width of GNR at the upper area is significantly modulated, relating to the electronic structure.[51]

In order to investigate the mechanism of the cleaning process/reaction between Si and Br atoms, we employed DFT simulations to explore the different stages. Figure 4a,b shows a comparison of the energetics of Si and Br configurations on the Au(111) surface. In general, our calculations demonstrate that, after the initial adsorption of Si and Br on the surface, energy is gained in every step toward forming $SiBr_4$ on the surface with the presence of highly mobile Br atoms facilitating the reaction stages.[19] However, if we also consider the binding energy of the configurations on the surface, we predict that $SiBr_4$ is bound by less than 1.2 eV and will desorb easily at 180 °C,[52] as seen in experiments. Furthermore, the kinetic energy of thermally evaporated Si atoms should assist in overcoming any activation energy barrier, leading to desorption even at room temperature. Besides Br atoms, we observed clusters with different sizes, which presumably correspond to $SiBr_x$ ($x = 0 - 4$).

In order to investigate the species of the $SiBr_x$ cluster, we simulated STM images for each structure as well as Si and Br atoms adsorbed on Au(111). We found that the individual Si atom should appear as a concave due to the depression of the conductivity, yet such a drip was not observed in the experiment (Figure 2). In order to investigate the contrast of
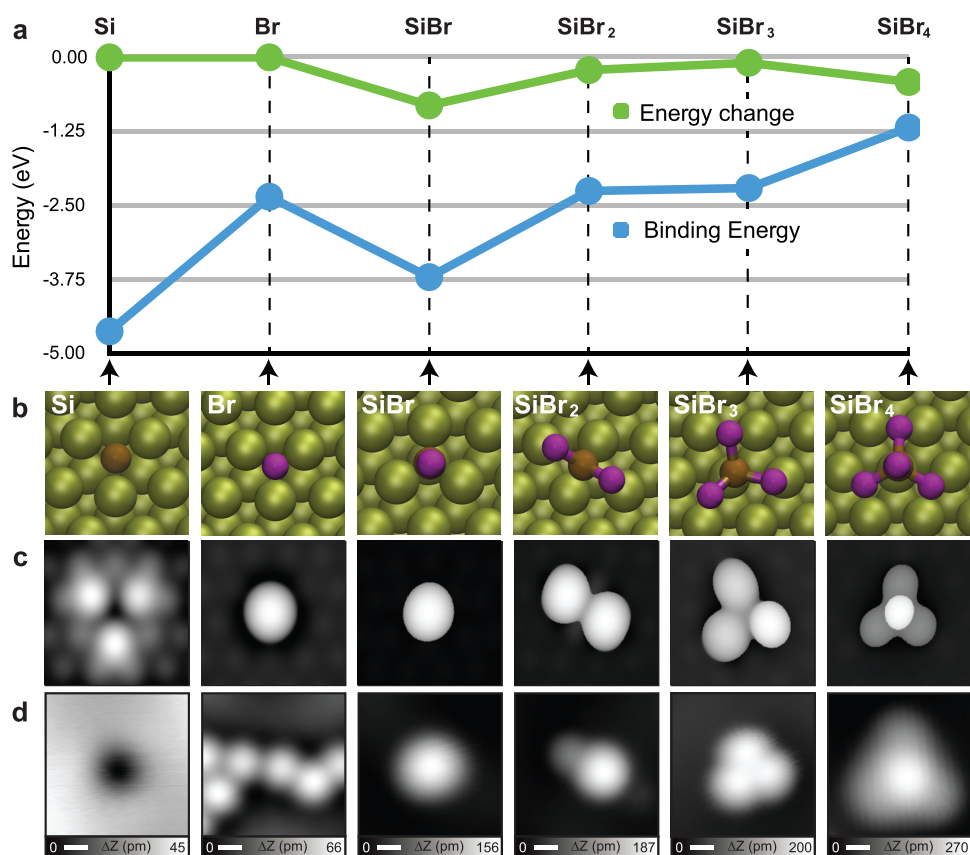
Figure 4. (a) Comparison of the energetics of the reaction processes of Si and Br atoms on the Au(111) surface. (b) Ground state adsorption structures on the surface. The plot shows both the binding energy of each system and also the change in energy when moving from one system to the next with reference to the energies of isolated Br atoms on the surface (isolated Si and Br atoms have zero energy change as no reaction has occurred). For example, forming SiBr results in a favorable energy gain of approximately 0.8 eV versus remaining as Si and an isolated Br on the surface. (c) Simulated STM images for each structure and (d) the corresponding STM topographies observed in the experiment. Scale bar: 300 pm.

a single Si atom adsorbed on Au(111), we deposited Si atoms on a clean Au(111). We found that most of Si atoms are condensed with each other and appear as wide depressions in the STM topography (Figure S4). Occasionally, we found a small dip, which is indeed in good agreement with that obtained in the STM simulation. Apparently, nearly all of the deposited Si atoms reacted to the Br atoms on the surface so that single Si atoms are absent in Figure 2. Therefore, the smallest cluster seen in Figure 3b corresponds to the SiBr molecule. In fact the apparent corrugation amplitude of the SiBr molecule is larger than the Br atom by 50 pm, which is in agreement with the calculations. The linear cluster adsorbed on the ripple of the herringbone structure appears asymmetric (Figure 2a) and is probably an $SiBr_2$ molecule based on comparison to simulations. Considering the fact that the STM simulation is conducted on a flat Au(111) surface, the asymmetric contrast most probably relates to the effect of the herringbone structure on the adsorption geometry.

Subsequently, the three-fold cluster corresponds to the $SiBr_3$ molecule (Figure 2c) and, while seen rarely, the $SiBr_4$ molecule is occasionally visible. For a comparison of the image contrast, the observed $SiBr_x$ molecules (x = 1,2,3,4) and Br atom in the experiment are shown in Figure 4d. Note that no individual Si atom on Au(111) is observed in the experiment if the Br atoms are a priori adsorbed. Nevertheless, since $SiBr_x$ (x = 1,2,3) molecules can be observed on Au(111) in the experiment, this suggests that their binding energies are higher than those of $SiBr_4$, corresponding to the results of simulations. The energy

diagram also indicates the population of each SiB_x species. We found that the SiBr molecule is the most abundant one (248 molecules) followed by $SiBr_2$ (19 molecules) and $SiBr_3$ (14 molecules) in a total area of 11,400 nm^2 after depositing Si atoms (Figure S5). Note that no $SiBr_4$ was found in the analyzed area. The order of populations is in agreement with the one for the binding energies (Figure 4a). After depositing more Si atoms and annealing at 180 °C, the numbers of the $SiBr_x$ are drastically reduced. While the number of molecules was not sufficient for the analysis (20 SiBr, 14 $SiBr_2$, 0 $SiBr_3$, and 2 $SiBr_4$ in a total area of 3100 nm^2), we still found more SiBr molecules than others.

■ IV. CONCLUSIONS

We present a technique to remove Br atoms from Au(111) at mild temperatures. Silicon atoms were deposited onto Au(111) after synthesis of n = 5 GNRs, which then react with the dissociated Br atoms, ultimately forming silicon tetrabromine molecules. Most of Br atoms can be removed at 180 °C due to the high volatility of tetrabromine, further supported by DFT calculations. Finally, most condensed GNRs become isolated without halogen pollution, making them much more suitable for detailed characterization. This method of on-surface purification may be further extended to the processes of fabricating nanostructures that need multistep chemical reactions.

■ ASSOCIATED CONTENT

Ⓢ Supporting Information

The Supporting Information is available free of charge at https://pubs.acs.org/doi/10.1021/acs.jpcc.0c06188.

Confined surface state by adsorbed Br atoms, GNRs with a large number of Br atoms, and the sample after being heated at high temperature (PDF)

■ AUTHOR INFORMATION

Corresponding Author

Shigeki Kawai − *Research Center for Advanced Measurement and Characterization, National Institute for Materials Science, Tsukuba, Ibaraki 305-0047, Japan; Graduate School of Pure and Applied Sciences, University of Tsukuba, Tsukuba 305-8571, Japan;* ⓘ orcid.org/0000-0003-2128-0120; Email: KAWAI.Shigeki@nims.go.jp

Authors

Kewei Sun − *Research Center for Advanced Measurement and Characterization, National Institute for Materials Science, Tsukuba, Ibaraki 305-0047, Japan*

Tomohiko Nishiuchi − *Department of Chemistry, Graduate School of Science, Osaka University, Toyonaka 560-0043, Japan;* ⓘ orcid.org/0000-0002-2113-0731

Keisuke Sahara − *Department of Chemistry, Graduate School of Science, Osaka University, Toyonaka 560-0043, Japan*

Takashi Kubo − *Department of Chemistry, Graduate School of Science, Osaka University, Toyonaka 560-0043, Japan;* ⓘ orcid.org/0000-0001-6809-7396

Adam S. Foster − *Department of Applied Physics, Aalto University School of Science, Espoo FI-00076, Finland; WPI Nano Life Science Institute (WPI-NanoLSI), Kanazawa University, Kanazawa 920-1192, Japan;* ⓘ orcid.org/0000-0001-5371-5905

Complete contact information is available at:
https://pubs.acs.org/10.1021/acs.jpcc.0c06188

Notes

The authors declare no competing financial interest.

■ ACKNOWLEDGMENTS

■ REFERENCES

(1) Grill, L.; Dyer, M.; Lafferentz, L.; Persson, M.; Peters, M. V.; Hecht, S. Nano-Architectures by Covalent Assembly of Molecular Building Blocks. *Nat. Nanotechnol.* **2007**, *2*, 687−691.

(2) Hla, S.-W.; Bartels, L.; Meyer, G.; Rieder, K.-H. Inducing All Steps of a Chemical Reaction with the Scanning Tunneling Microscope Tip: Towards Single Molecule Engineering. *Phys. Rev. Lett.* **2000**, *85*, 2777−2780.

(3) Bieri, M.; Treier, M.; Cai, J.; Aït-Mansour, K.; Ruffieux, P.; Gröning, O.; Gröning, P.; Kastler, M.; Rieger, R.; Feng, X.; et al. Porous Graphenes: Two-Dimensional Polymer Synthesis with Atomic Precision. *Chem. Commun.* **2009**, *45*, 6919−6921.

(4) Schuler, B.; Fatayer, S.; Mohn, F.; Moll, N.; Pavliček, N.; Meyer, G.; Peña, D.; Gross, L. Reversible Bergman Cyclization by Atomic Manipulation. *Nat. Chem.* **2016**, *8*, 220−224.

(5) Sun, Q.; Zhang, C.; Li, Z.; Kong, H.; Tan, Q.; Hu, A.; Xu, W. On-Surface Formation of One-Dimensional Polyphenylene through Bergman Cyclization. *J. Am. Chem. Soc.* **2013**, *135*, 8448−8451.

(6) Zhang, Y.-Q.; Kepčija, N.; Kleinschrodt, M.; Diller, K.; Fischer, S.; Papageorgiou, A. C.; Allegretti, F.; Björk, J.; Klyatskaya, S.; Klappenberger, F.; et al. Homo-Coupling of Terminal Alkynes on a Noble Metal Surface. *Nat. Commun.* **2012**, *3*, 1286.

(7) Gao, H.-Y.; Wagner, H.; Zhong, D.; Franke, J.-H.; Studer, A.; Fuchs, H. Glaser Coupling at Metal Surfaces. *Angew. Chem., Int. Ed.* **2013**, *52*, 4024−4028.

(8) Kawai, S.; Krejčí, O.; Foster, A. S.; Pawlak, R.; Xu, F.; Peng, L.; Orita, A.; Meyer, E. Diacetylene Linked Anthracene Oligomers Synthesized by One-Shot Homocoupling of Trimethylsilyl on Cu(111). *ACS Nano* **2018**, *12*, 8791−8797.

(9) Kanuru, V. K.; Kyriakou, G.; Beaumont, S. K.; Papageorgiou, A. C.; Watson, D. J.; Lambert, R. M. Sonogashira Coupling on an Extended Gold Surface in Vacuo: Reaction of Phenylacetylene with Iodobenzene on Au(111). *J. Am. Chem. Soc.* **2010**, *132*, 8081−8086.

(10) Shi, K.-J.; Shu, C.-H.; Wang, C.-X.; Wu, X.-Y.; Tian, H.; Liu, P.-N. On-Surface Heck Reaction of Aryl Bromides with Alkene on Au(111) with Palladium as Catalyst. *Org. Lett.* **2017**, *19*, 2801−2804.

(11) Weigelt, S.; Busse, C.; Bombis, C.; Knudsen, M. M.; Gothelf, K. V.; Strunskus, T.; Wöll, C.; Dahlbom, M.; Hammer, B.; Lægsgaard, E.; et al. Covalent Interlinking of an Aldehyde and an Amine on a Au(111) Surface in Ultrahigh Vacuum. *Angew. Chem., Int. Ed.* **2007**, *46*, 9227−9230.

(12) Zwaneveld, N. A. A.; Pawlak, R.; Abel, M.; Catalin, D.; Gigmes, D.; Bertin, D.; Porte, L. Organized Formation of 2D Extended Covalent Organic Frameworks at Surfaces. *J. Am. Chem. Soc.* **2008**, *130*, 6678−6679.

(13) Zhong, D.; Franke, J.-H.; Podiyanachari, S. K.; Blömker, T.; Zhang, H.; Kehr, G.; Erker, G.; Fuchs, H.; Chi, L. Linear Alkane Polymerization on a Gold Surface. *Science* **2011**, *334*, 213−216.

(14) Treier, M.; Pignedoli, C. A.; Laino, T.; Rieger, R.; Müllen, K.; Passerone, D.; Fasel, R. Surface-Assisted Cyclodehydrogenation Provides a Synthetic Route Towards Easily Processable and Chemically Tailored Nanographenes. *Nat. Chem.* **2011**, *3*, 61−67.

(15) Gao, H.-Y.; Held, P. A.; Knor, M.; Mück-Lichtenfeld, C.; Neugebauer, J.; Studer, A.; Fuchs, H. Decarboxylative Polymerization of 2,6-Naphthalenedicarboxylic Acid at Surfaces. *J. Am. Chem. Soc.* **2014**, *136*, 9658−9663.

(16) Cai, J.; Ruffieux, P.; Jaafar, R.; Bieri, M.; Braun, T.; Blankenburg, S.; Muoth, M.; Seitsonen, A. P.; Saleh, M.; Feng, X.; et al. Atomically Precise Bottom-Up Fabrication of Graphene Nanoribbons. *Nature* **2010**, *466*, 470−473.

(17) Otero, G.; Biddau, G.; Sánchez-Sánchez, C.; Caillard, R.; López, M. F.; Rogero, C.; Palomares, F. J.; Cabello, N.; Basanta, M. A.; Ortega, J.; et al. Fullerenes from Aromatic Precursors by Surface-Catalysed Cyclodehydrogenation. *Nature* **2008**, *454*, 865−868.

(18) Lafferentz, L.; Eberhardt, V.; Dri, C.; Africh, C.; Comelli, G.; Esch, F.; Hecht, S.; Grill, L. Controlling On-Surface Polymerization by Hierarchical and Substrate-Directed Growth. *Nat. Chem.* **2012**, *4*, 215−220.

(19) Björk, J.; Hanke, F.; Stafström, S. Mechanisms of Halogen-Based Covalent Self-Assembly on Metal Surfaces. *J. Am. Chem. Soc.* **2013**, *135*, 5768−5775.

(20) de Oteyza, D. G.; García-Lekue, A.; Vilas-Varela, M.; Merino-Díez, N.; Carbonell-Sanromá, E.; Corso, M.; Vasseur, G.; Rogero, C.; Guitián, E.; Pascual, J. I.; et al. Substrate-Independent Growth of Atomically Precise Chiral Graphene Nanoribbons. *ACS Nano* **2016**, *10*, 9000−9008.

(21) Lafferentz, L.; Ample, F.; Yu, H.; Hecht, S.; Joachim, C.; Grill, L. Conductance of a Single Conjugated Polymer as a Continuous Function of Its Length. *Science* **2009**, *323*, 1193−1197.

(22) Giovannantonio, M. D.; Deniz, O.; Urgel, J. I.; Widmer, R.; Dienel, T.; Stolz, S.; Sánchez-Sánchez, C.; Muntwiler, M.; Dumslaff,

T.; Berger, R.; et al. On-Surface Growth Dynamics of Graphene Nanoribbons: The Role of Halogen Functionalization. *ACS Nano* **2018**, *12*, 74−81.

(23) Kawai, S.; Sadeghi, A.; Okamoto, T.; Mitsui, C.; Pawlak, R.; Meier, T.; Takeya, J.; Goedecker, S.; Meyer, E. Organometallic Bonding in an Ullmann-Type On-Surface Chemical Reaction Studied by High-Resolution Atomic Force Microscopy. *Small* **2016**, *12*, 5303−5311.

(24) Bieri, M.; Nguyen, M.-T.; Gröning, O.; Cai, J.; Treier, M.; Aït-Mansour, K.; Ruffieux, P.; Pignedoli, C. A.; Passerone, D.; Kastler, M.; et al. Two-Dimensional Polymer Formation on Surfaces: Insight into the Roles of Precursor Mobility and Reactivity. *J. Am. Chem. Soc.* **2010**, *132*, 16669−16676.

(25) Batra, A.; Cvetko, D.; Kladnik, G.; Adak, O.; Cardoso, C.; Ferretti, A.; Prezzi, D.; Molinari, E.; Morgante, A.; Venkataraman, L. Probing the Mechanism for Graphene Nanoribbon Formation on Gold Surfaces through X-ray Spectroscopy. *Chem. Sci.* **2014**, *5*, 4419−4423.

(26) Fan, Q.; Wang, C.; Liu, L.; Han, Y.; Zhao, J.; Zhu, J.; Kuttner, J.; Hilt, G.; Gottfried, J. M. Covalent, Organometallic, and Halogen-Bonded Nanomeshes from Tetrabromo-Terphenyl by Surface-Assisted Synthesis on Cu(111). *J. Phys. Chem. C* **2014**, *118*, 13018−13025.

(27) Vasseur, G.; Fagot-Revurat, Y.; Sicot, M.; Kierren, B.; Moreau, L.; Malterre, D.; Cardenas, L.; Galeotti, G.; Lipton-Duffin, J.; Rosei, F.; et al. Quasi One-Dimensional Band Dispersion and Surface Metallization in Long-Range Ordered polymeric wires. *Nat. Commun.* **2016**, *7*, 10235.

(28) Merino-Díez, N.; Lobo-Checa, J.; Nita, P.; Garcia-Lekue, A.; Basagni, A.; Vasseur, G.; Tiso, F.; Sedona, F.; Das, P. K.; Fujii, J.; et al. Switching from Reactant to Substrate Engineering in the Selective Synthesis of Graphene Nanoribbons. *J. Phys. Chem. Lett.* **2018**, *9*, 2510−2517.

(29) Simonov, K. A.; Vinogradov, N. A.; Vinogradov, A. S.; Generalov, A. V.; Zagrebina, E. M.; Mårtensson, N.; Cafolla, A. A.; Carpy, T.; Cunniffe, J. P.; Preobrajenski, A. B. Effect of Substrate Chemistry on the Bottom-Up Fabrication of Graphene Nanoribbons: Combined Core-Level Spectroscopy and STM Study. *J. Phys. Chem. C* **2014**, *118*, 12532−12540.

(30) Bronner, C.; Björk, J.; Tegeder, P. Tracking and Removing Br during the On-Surface Synthesis of a Graphene Nanoribbon. *J. Phys. Chem. C* **2015**, *119*, 486−493.

(31) Chen, Y.-C.; de Oteyza, D. G.; Pedramrazi, Z.; Chen, C.; Fischer, F. R.; Crommie, M. F. Tuning the Band Gap of Graphene Nanoribbons Synthesized from Molecular Precursors. *ACS Nano* **2013**, *7*, 6123−6128.

(32) Kawai, S.; Saito, S.; Osumi, S.; Yamaguchi, S.; Foster, A. S.; Spijker, P.; Meyer, E. Atomically Controlled Substitutional Boron-Doping of Graphene Nanoribbons. *Nat. Commun.* **2015**, *6*, 8098.

(33) Ruffieux, P.; Wang, S.; Yang, B.; Sánchez-Sánchez, C.; Liu, J.; Dienel, T.; Talirz, L.; Shinde, P.; Pignedoli, C. A.; Passerone, D.; et al. On-Surface Synthesis of Graphene Nanoribbons with Zigzag Edge Topology. *Nature* **2016**, *531*, 489−492.

(34) Zhang, H.; Lin, H.; Sun, K.; Chen, L.; Zagranyarski, Y.; Aghdassi, N.; Duhm, S.; Li, Q.; Zhong, D.; Li, Y.; et al. On-Surface Synthesis of Rylene-Type Graphene Nanoribbons. *J. Am. Chem. Soc.* **2015**, *137*, 4022−4025.

(35) Dienel, T.; Kawai, S.; Söde, H.; Feng, X.; Müllen, K.; Ruffieux, P.; Fasel, R.; Gröning, O. Resolving Atomic Connectivity in Graphene Nanostructure Junctions. *Nano Lett.* **2015**, *15*, 5185−5190.

(36) Abyazisani, M.; MacLeod, J. M.; Lipton-Duffin, J. Cleaning Up after the Party: Removing the Byproducts of On-Surface Ullmann Coupling. *ACS Nano* **2019**, *13*, 9270−9278.

(37) Kresse, G.; Furthmüller, J. Efficiency of ab-initio Total Energy Calculations for Metals and Semiconductors Using a Plane-Wave Basis Set. *Comp. Mat. Sci.* **1996**, *6*, 15−50.

(38) Kresse, G.; Furthmüller, J. Efficient Iterative Schemes for *ab initio* Total-Energy Calculations Using a Plane-Wave Basis Set. *Phys. Rev. B* **1996**, *54*, 11169−11186.

(39) Tkatchenko, A.; DiStasio, R. A., Jr.; Car, R.; Scheffler, M. Accurate and Efficient Method for Many-Body van der Waals Interactions. *Phys. Rev. Lett.* **2012**, *108*, 236402.

(40) Ambrosetti, A.; Reilly, A. M.; DiStasio, R. A., Jr.; Tkatchenko, A. Long-Range Correlation Energy Calculated from Coupled Atomic Response Functions. *J. Chem. Phys.* **2014**, *140*, 18A508.

(41) Blochl, P. E. Projector Augmented-Wave Method. *Phys. Rev. B* **1994**, *50*, 17953−17979.

(42) Migani, A.; Illas, F. A Systematic Study of the Structure and Bonding of Halogens on Low-Index Transition Metal Surfaces. *J. Phys. Chem. B* **2006**, *110*, 11894−11906.

(43) Zhu, Q.; Wang, S.-q. Trends and Regularities for Halogen Adsorption on Various Metal Surfaces. *J. Electrochem. Soc.* **2016**, *163*, H796−H808.

(44) Humphrey, W.; Dalke, A.; Schulten, K. VMD: Visual Molecular Dynamics. *J. Mol. Graphics* **1996**, *14*, 33−38.

(45) Vanpoucke, D. E. P.; Brocks, G. Formation of Pt-Induced Ge Atomic Nanowires on Pt/Ge(001): A Density Functional Theory Study. *Phys. Rev. B* **2008**, *77*, 241308.

(46) Tersoff, J.; Hamann, D. R. Theory of the Scanning Tunneling Microscope. *Phys. Rev. B* **1985**, *31*, 805−813.

(47) Pham, T. A.; Song, F.; Nguyen, M.-T.; Li, Z.; Studener, F.; Stöhr, M. Comparing Ullmann Coupling on Noble Metal Surfaces: On-Surface Polymerization of 1,3,6,8-Tetrabromopyrene on Cu(111) and Au(111). *Chem. − Eur. J.* **2016**, *22*, 5937−5944.

(48) Nanayakkara, S. U.; Sykes, E. C. H.; Fernández-Torres, L. C.; Blake, M. M.; Weiss, P. S. Long Range Electronic Interactions at a High Temperature: Bromine Adatom Islands on Cu(111). *Phys. Rev. Lett.* **2007**, *98*, 206108.

(49) Kawai, S.; Takahashi, K.; Ito, S.; Pawlak, R.; Meier, T.; Spijker, P.; Canova, F. F.; Tracey, J.; Nozaki, K.; Foster, A. S.; et al. Competing Annulene and Radialene Structures in a Single Anti-Aromatic Molecule Studied by High-Resolution Atomic Force Microscopy. *ACS Nano* **2017**, *11*, 8122−8130.

(50) Deniz, O.; Sánchez-Sánchez, C.; Dumslaff, T.; Feng, X.; Narita, A.; Müllen, K.; Kharche, N.; Meunier, V.; Fasel, R.; Ruffieux, P. Revealing the Electronic Structure of Silicon Intercalated Armchair Graphene Nanoribbons by Scanning Tunneling Spectroscopy. *Nano Lett.* **2017**, *17*, 2197−2203.

(51) Kimouche, A.; Ervasti, M. M.; Drost, R.; Halonen, S.; Harju, A.; Joensuu, P. M.; Sainio, J.; Liljeroth, P. Ultra-Narrow Metallic Armchair Graphene Nanoribbons. *Nat. Commun.* **2015**, *6*, 10177.

(52) Wang, K.-T.; Nachimuthu, S.; Jiang, J.-C. Temperature-Programmed Desorption Studies of NH_3 and H_2O on the RuO_2(110) Surface: Effects of Adsorbate Diffusion. *Phys. Chem. Chem. Phys.* **2018**, *20*, 24201−24209.